Polymer Testing 124 (2023) 108084

Contents lists available at ScienceDirect

Polymer Testing

journal homepage: www.elsevier.com/locate/polytest

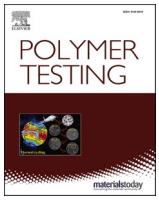

High-temperature creep behaviors of polybutene-1 with different chain microstructure and molecular weight

Yuanjin Zhao, Chenguang Liu, Huafeng Shao, Aihua He *

Shandong Provincial Key Laboratory of Olefin Catalysis and Polymerization, Key Laboratory of Rubber-Plastics (Ministry of Education), School of Polyme Sciecne and Engineering, Qingdao University of Science and Technology, Qingdao, 266042, China

ARTICLE INFO

Keywords:
Polybutene-1
Ziegler-Natta catalyst
Stereoregularity
Molecular weight
High temperature creep

ABSTRACT

The creep resistance of polymer determines the dimensional stability of product under stress. The isotactic polybutene-1 (*i*PB) with outstanding high-temperature creep resistance and stress-crack resistance is applied widely in the field of hot-water pipes. Although the chain information including weight-average molecular weight (M_w) and aggregate structures of isotactic polybutene-1 (*i*PB) influence the creep resistance, the crucial factor affecting the creep behavior greatly is unclear. In this work, a series PB samples with varied M_w, isotacticity and configurational sequence were synthesized and characterized based on Gel Permeation Chromatography (GPC), solvent fractionation and Nuclear Magnetic Resonance Spectroscopy (NMR). The Differential Scanning Calorimetry (DSC), Wide-angle X-ray diffraction (WAXD) and Small angle X-ray scattering (SAXS) were used to characterize the aggregation structures of PB samples. The stress-strain behaviors and 95 °C creep deformation of these PB samples were testes by tensile test and Dynamic Mechanical Analysis (DMA), respectively. It was found that these PB samples showed different chain microstructures like 88–99 *wt*% high isotactic PB (H*i*PB) fractions, 90–97.6 mol% tetra-meso placements (mmmm) in H*i*PB fraction, and 50×10^4-160×10^4 M_w. Increasing the molecular weight, isotacticity or configurational sequence mmmm enhanced the creep resistance of PB, while mmmm configurational sequence played more important role in creep resistance of PB through adjusting the aggregation structure (crystalline domains) of the final product greatly. Exploring the influencing factors of creep resistance provided guidance for the synthesis of high-performance PB for high-temperature pipe application.

1. Introduction

Polymer creep, as time and temperature dependent phenomenon, reflects the increase in deformation of a polymer with time extension under the action of stress. Due to the viscoelastic nature of polymers, the creep phenomenon is unavoidable [1]. This dimensional stability of the polymers becomes worse at high temperature and results in irreversible damage to the materials. The creep resistance is crucial for high-temperature pipe application. Polymer materials like polyethylene (PE-RT) [2–4], cross-linked polyethylene (PE-X), random copolymerized propylene (PP-R) [5–7] and polybutene-1 (PB) [8–10] are generally used for geothermal heating in residences, hotels and other places. Among those materials, PB with excellent creep resistance, as well as excellent resistance to environmental stress cracking and high temperature shock resistance, attracted much attentions in both industry and academics.

The creep behaviors of polymers might be affected by the molecular weight [11–13] and aggregate structure [11,14,15] of the polymer products, which might also be influenced by the application conditions like applied stress [16,17], temperature [17–20], time, relative humidity [21] and ultraviolet rays [22]. Bhateja [11] and O'Connell [12] proposed that increasing molecular weight could improve the creep performance of Polyethylene (PE). Handge et al. [13] found that the creep resistance of polystyrene-*block*-poly (methyl methacrylate) (PS-*b*-PMMA) increased gradually with the increase in its molecular weight based on the decrease in creep compliance. Ruan [14] and Bhattacharyya [15] changed the crystallinity of the polymer by adding fillers to the polymer, thus changing the creep performance of the polymer.

PB, as a special polymorphic polyolefin material [23–25], has the peculiar crystal-crystal transformation under room temperature [26–32] from unstable form II to stable form I. The outstanding creep resistance

* Corresponding author.
E-mail addresses: aihuahe@iccas.ac.cn, ahhe@qust.edu.cn (A. He).

https://doi.org/10.1016/j.polymertesting.2023.108084
Received 29 March 2023; Received in revised form 15 May 2023; Accepted 25 May 2023
Available online 26 May 2023

Table 1
Chain structures and physical-mechanical properties of PB.

Sample	M_w (× 10^4)	MWD	Chain microstructure		Chain entanglement[b]			Aggregate structure				MFR (g/10min)	Mechanical properties				
			HiPB Fractions (wt%)	mmmm[a] (mol%)	*E* (MPa)	M_e (kg/mol)	ν_e (mol/m^3)	T_m[c] (°C)	X_c[c] (%)	d_c[d] (nm)	F_f[e] (%)		Tensile strength (MPa)	High temperature creep @95 °C[f]			
														Creep deformation (ε, %)	ε_E (%)	ε_V (%)	ε_∞ (%)
PB-1	51	6.8	92.7	97.6	0.07	0.13	6.80	134	41.8	17.2	98.1	2.6	32.1 ± 0.8	6.2	4.6	0.2	1.4
PB-2	51	6.5	91.5	92.2	0.09	0.11	8.45	133	37.1	16.6	99.2	2.1	30.1 ± 1.1	9.0	6.6	0.6	1.8
PB-3	57	7.4	88.3	90.1	0.08	0.12	7.68	131	36.5	16.0	96.6	1.8	25.4 ± 1.2	9.6	7.0	0.6	2.0
PB-4	70	6.8	95.8	90.1	0.13	0.07	12.06	129	36.9	15.4	96.0	1.2	33.3 ± 0.4	9.2	6.9	0.7	1.6
PB-5	137	5.4	95.6	93.9	0.29	0.03	28.06	130	36.9	19.1	96.0	0.2	33.3 ± 1.9	7.7	5.8	0.4	1.5
PB-6	157	6.5	89.7	–	0.41	0.02	39.48	131	28.0	16.9	93.7	0.1	27.0 ± 2.0	15.5	12.9	1.2	1.4
PB-C	77	4.2	99.0	92.2	0.12	0.08	11.14	130	41.1	18.3	96.2	0.5	34.7 ± 1.0	8.0	5.7	0.5	1.8

[a] The fully isotactic mmmm pentads concentration (mmmm, mol%) of the HiPB fraction.
[b] Measured by DMA.
[c] T_m and X_c are the melting point and crystallinity of PB (form I).
[d] The lamellar thickness (d_c) is tested by SAXS.
[e] The fraction of PB form I (F_I) is tested by WAXD.
[f] Obtained from DMA.

of PB was attributed to the form I crystals with immobile polymer backbone, slowly reoriented ethyl groups without changes of their conformational state, high lamellar thickness and high crystallinity [33]. Previously, some scholars have reported the influence of the molecular weight of PB on rheological properties [10,34,35] and crystallization behavior [26,36], and the influence of the aggregate structure on mechanical properties [37,38] such as tensile properties, impact strength and density. The crucial factor which determines the creep behavior of PB is rarely reported.

In this work, 6 kinds of *i*PB samples with different molecular weight, varied isotacticity and varied configurational sequence were synthesized by using Ziegler-Natta catalyst under various polymerization conditions. The isotacticity was characterized with Hi*i*PB fraction percentage by solvent fractionation method, and the configurational sequence was characterized with mmmm concentration from ^{13}C-NMR spectra. The effects of molecular weight, isotacticity and configurational sequence on the aggregation structures and then high-temperature creep resistance of PB (form I) were investigated. This work aims to provide theoretical guidance for the production of hot water pipes with excellent high-temperature creep properties by exploring the structures of PB molecular chains.

2. Experimental

2.1. Materials

The PB samples (PB-1∼PB-6) were synthesized by Ziegler-Natta catalyst in our laboratory. PB-C were commercial PB product (PB4253) for pipe application. Other reagents, such as xylene, *n*-pentane and absolute ethanol, were commercial agents and used without further purification.

2.2. Fractionation of PB

2 g PB sample was completely dissolved in 200 ml boiling xylene, then the PB solution was annealed at −20 °C for 24 h before filtration and separation for xylene soluble (xyl-sol) fractions and xylene insoluble (xyl-ins) fractions. The xyl-sol fractions were dried in a vacuum at 40 °C for 24 h and then extracted with boiling *n*-pentane for another 24 h to obtain *n*-pentane soluble (C5-sol) fractions and *n*-pentane insoluble (C5-ins) fractions. All those fractions including xyl-sol, C5-sol, C5-ins representing atactic PB (*a*PB), medium isotactic PB (Mi*i*PB), high isotactic polybutene-1 (Hi*i*PB) [39], respectively, were vacuum dried at 40 °C till constant weight were reached. The Hi*i*PB percentage was donated as isotacticity of PB.

2.3. Specimens for physical and mechanical tests

The PB-1 to PB-6 specimens in the form of sheets were prepared by compression molding of PB powers at 190 °C under 10 MPa for 5 min.

The commercial PB specimens were prepared by compression molding of PB pellets at 190 °C under 10 MPa for 5min.

All above PB sheets were annealed at room temperature for at least 7 days before testing to complete the transition from form II to form I.

2.4. Characterizations

The weight-average molecular weight (M_w) and molecular weight distribution (MWD) of PB were tested by Waters GPC 2000 with 1,2,4-trichlorobenzene as solvent at 150 ± 0.05 °C, and calibrated with polystyrene standard samples. The GPC curves was deconvoluted into different Flory components by Flory peak fitting.

The DSC test was carried out with PerkinElmer DSC 8500 under a nitrogen atmosphere, which was calibrated with Indium. 5–10 mg samples were heated from 30 °C to 200 °C at the rate of 10 °C/min, and the heating curves were recorded to calculate the crystallinity (X_c) of PB

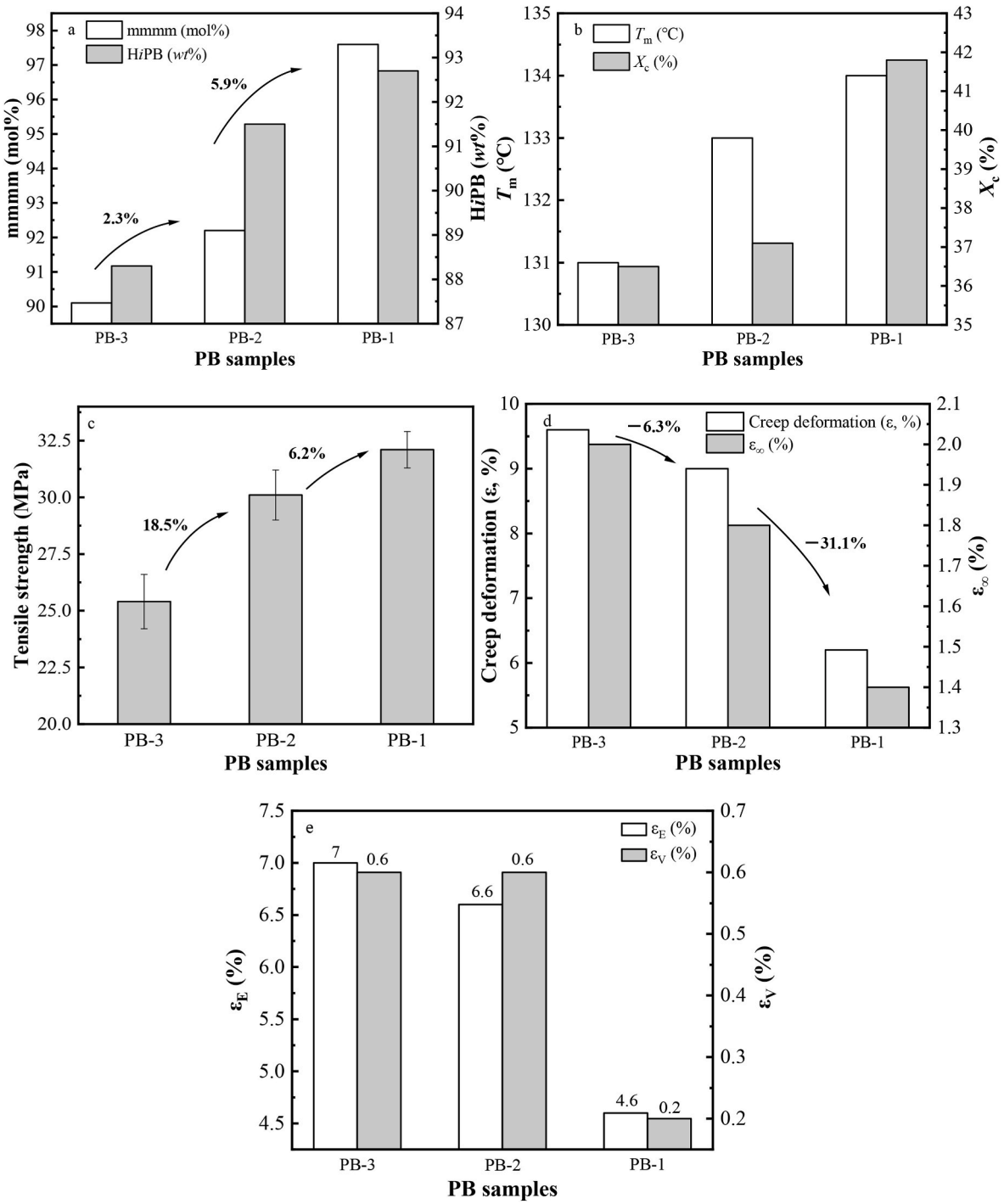

Fig. 1. (a)Percentages of mmmm and H*i*PB fraction; (b)T_m and X_c; (c)tensile strength; (d)creep deformation (ε) and permanent creep strain (ε_∞); (e)elastic creep strain (ε_E) and viscoelastic portion of the strain (ε_V) of PB samples with similar molecular weight.

according to formula (1).

$$X_c(\%) = \frac{\Delta H_m}{\Delta H_f^*} \times 100\% \quad (1)$$

ΔH_m is the melting enthalpy obtained in DSC test, and ΔH_f^* is the melting enthalpy of complete crystallization of PB (form I, 141 J/g [30]).

Bruker AVANCE III spectrometer was used for ^{13}C-NMR test with 1,2-dichlorobenzene-d4 as solvent. The test temperature was 120 °C and the scanning times were 3000–5000.

Wide-angle X-ray diffraction (WAXD) measurements were performed using a Xenocs France diffractometer with Cu-Kα radiation (λ = 0.154 nm). The distances between samples to detector was 172 nm and the exposure time was 60 s. Two-dimensional images were recorded by a Pilatus 300 K detector. The fraction of form I (F_I) was calculated by formula (2) [40].

$$F_I = \frac{I(110)_I}{I(110)_I + 0.67I(200)_{II}} \quad (2)$$

The long-period (d_{ac}), lamellar thickness (d_c) and amorphous thickness (d_a) of PB samples were measured by Small angle X-ray scattering (SAXS) technique (Xeuss of Xenocs, France). The distance between the

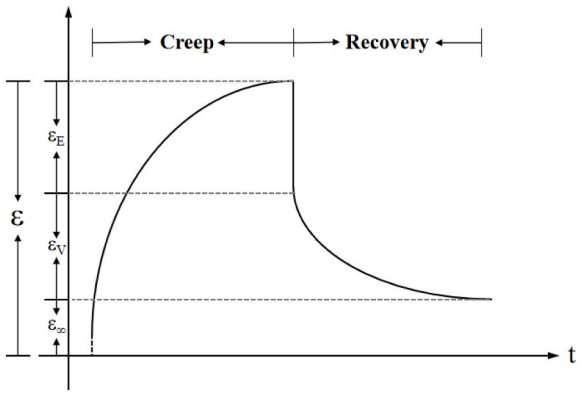

Fig. 2. Schematic diagram of a creep-recovery test.

sample and the detector is 2430 mm, and the X-ray wavelength is 0.154 nm. The scattering pattern was collected within 120 s, and the background is corrected and normalized by standard procedures. The fitting electron density correlation function $K(z)$ can be derived from the inverse Fourier transform of the experimental intensity distribution $I(q)$:

$$K(z) = \frac{\int_0^\infty I(q)q^2 \cos(qz)dq}{\int_0^\infty I(q)q^2 dq} \tag{3}$$

where z represents the position measured along the trajectory perpendicular to the surface of the layered body, and the multiplication of $I(q)$ and q^2 (Lorentz correction) is performed. The specific structural parameters d_{ac}, d_c and d_a are calculated by correlation function.

The melt flow rate of the sample was tested according to GB/T-3682-2000 at 190 °C under 2.16 kg with Melt flow rate meter (CT-7100-MI, High Speed Rail Technology Co., Ltd.).

The stress-strain curves of PB samples were tested with Zwick/Roell Z005 BET-TC02.00 (Zwick, Germany) electrical tensile tester at (25 ± 2) °C according to GB/T1040 with a cross-section traction speed of 50 mm/min.

The thermal creep properties of PB samples were tested by DMA (DMA+1000, Metravib, France). The creep time was 4 h, the ambient temperature was 95 °C, and the test stress was 8 MPa. After reaching the set time, the stress was released to 0 MPa and specimen was relaxed for 10 min.

The molecular weight between entanglements (M_e, kg/mol) and the average molecular entanglement density (v_e, mol/m^3) of PB samples were obtained by DMA (DMA Q800, TA, America) at a heating rate of 1 °C/min in the range of 30 °C–160 °C with a frequency of 1 Hz. The M_e was obtained based on equation (4), [41–43].

$$E = 3\rho RT/M_e \tag{4}$$

Where E (MPa) is the elastic modulus at 145 °C in the flat region of the DMA curve; ρ (kg/m^3) is the density of *i*PB; R is the gas constant, the value is 8.314 J/(K/mol); T (K) is the absolute temperature at 145 °C. The average molecular entanglement density (v_e, mol/m^3) is calculated by equation (5).

$$v_e = \rho/M_e \tag{5}$$

IBM SPSS Statistics 25 was used for data fitting to establish linear relationship between creep deformation and variates including configurational sequence and M_w.

3. Results and discussion

A series of PB samples were synthesized with $TiCl_4/MgCl_2$ type Ziegler-Natta catalyst in 1 L autoclave under various conditions in our laboratory [44–46]. These samples were subjected to structural characterization, thermal creep and tensile tests, and the results were shown in Table 1.

3.1. Influence of PB chain microstructure

Based on GPC and DMA measurements, PB-1, PB-2 and PB-3 were proved to have similar M_w, very close average molecular entanglement density (v_e) and molecular weight between entanglements (M_e) (Table 1). The fully isotactic mmmm pentads (mmmm) concentration (mol%) and high isotactic PB (H*i*PB) fraction percentage (*wt* %) were used to indicate the configurational sequence and isotacticity of PB samples, respectively. As Fig. 1a and Table 1 shown, the isotacticity of PB-3, PB-2, PB-1 increased gradually from 88.3% to 92.7%. While the mmmm concentration of PB-3, PB-2, PB-1 increased gradually from 90.1% to 97.6%. The mmmm concentration and H*i*PB fraction percentage for PB-1 were 97.6% and 92.7%, respectively. The increase in mmmm concentration and H*i*PB fraction of PB chains resulted in obviously increase in crystallization melting temperature (T_m), crystallinity (X_c) (Fig. 1b) and the lamellar thickness (d_c). For PB-1 sample, the T_m reached as high as 134 °C (3 °C higher than PB-3), the X_c reached as high as 41.8% (5.3% higher than PB-3) (Fig. 1b) and the d_c as high as 17.2 nm (1.2 nm higher than PB-3) (Table 1).

The creep tests of PB samples were carried out at 95 °C under 8 MPa measured by DMA. The classical creep-recovery curve was shown in Fig. 2 [47,48], and the creep deformation (ε, %) could be described by equation (6):

$$\varepsilon = \varepsilon_E + \varepsilon_V + \varepsilon_\infty \tag{6}$$

Where ε_E (%) is the elastic creep strain, ε_V (%) is the viscoelastic portion of the strain and ε_∞ (%) is the permanent creep strain.

The increase in chain stereoregularity of PB resulted in obviously increased tensile strength (Fig. 1c), greatly reduced creep deformation at 95 °C and sharply decreased permanent creep strain (Fig. 1d). Compared with PB-3 with mmmm = 90.1%, PB-1 with mmmm = 97.6% had more perfect crystals (form I with d_c = 17.2 nm) showing the highest crystallinity (41.8%) and the highest T_m (134 °C, form I), which acted as the rigid physical crosslinking points in the polymer matrix to reduce the slip of molecular chains at high temperature, and then contributed to the lowest creep deformation at 95 °C (6.2%). The glass transition temperature (T_g) of PB was about −25 °C [30], so the crystalline domains and amorphous domains in PB were in the crystalline state and the high-elastic state at 95 °C, respectively. PB-1 with the highest X_c and relatively high F_I showed the lest profound viscoelastic behavior when compared to PP-2 and PB-3, and presented the lowest ε_V and ε_E values (Fig. 1e).

3.2. Influence of PB molecular weight

The PB-3 and PB-4 pair with similar mmmm concentration (mmmm = 90%) and varied M_w (57×10^4 vs 70×10^4), and PB-2 and PB-5 pair with similar mmmm concentration (mmmm = 92–93%) and varied M_w (51×10^4 vs 137×10^4), were selected to study the influences of molecular weight on creep behavior of PB samples (Fig. 3a). The v_e values of PB-3, PB-4, PB-2 and PB-5 were 7.68, 12.06, 8.45, 28.06 mol/m^3, respectively. Based on the Flory peak-spiltting and fitting, the distribution of fractions with varied molecular weight in each PB sample was shown in Fig. 3b. For both PB-3 and PB-4 pair, and PB-2 and PB-5 pair, the main fractions showed M_w in the range of 20–100 $\times 10^4$, and both PB-3 and PB-2 had relatively high low-M_w fraction content. While PB-5 possessed extremely high M_w, and about 30% fractions with M_w in the range of 100–200 $\times 10^4$ and 15% fractions with M_w larger than 200 $\times 10^4$. The variation of M_w in PB had little influence on T_m and X_c of PB samples indicated those PB samples had similar aggregation structures (Table 1, Fig. 3c). The PB-3 and PB-4 with similar crystallinity showed few changes in ε_E and ε_V values (Fig. 3f), while the increase in M_w of PB-4 led to an increase in tensile strength (Fig. 3d) and an obvious decrease

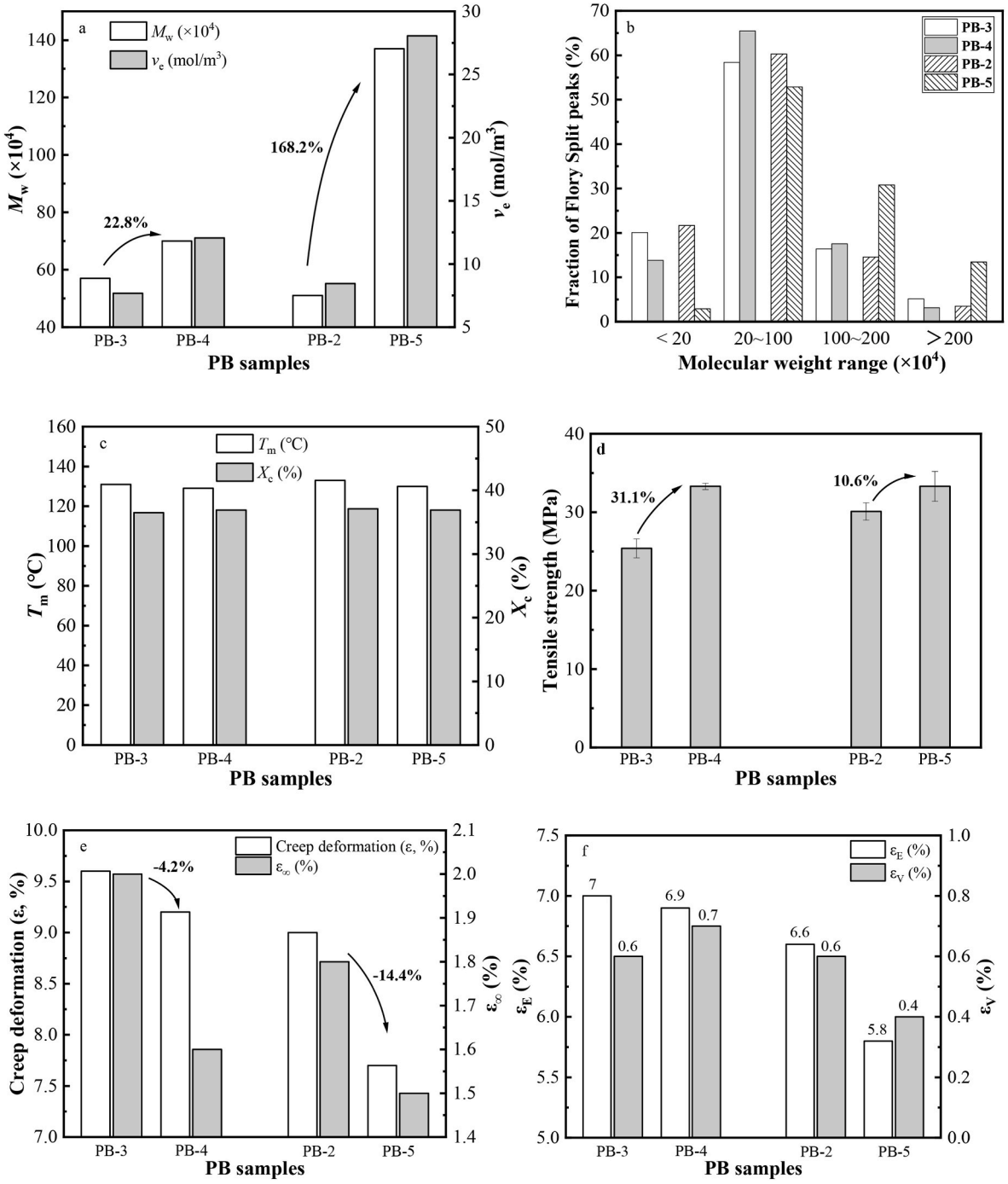

Fig. 3. (a)M_w and v_e; (b)the fraction of Flory split peaks; (c)T_m and X_c; (d)tensile strength; (e)creep deformation and permanent creep strain; (f)elastic creep strain (ε_E) and viscoelastic portion of the strain (ε_V) of PB with similar mmmm concentration.

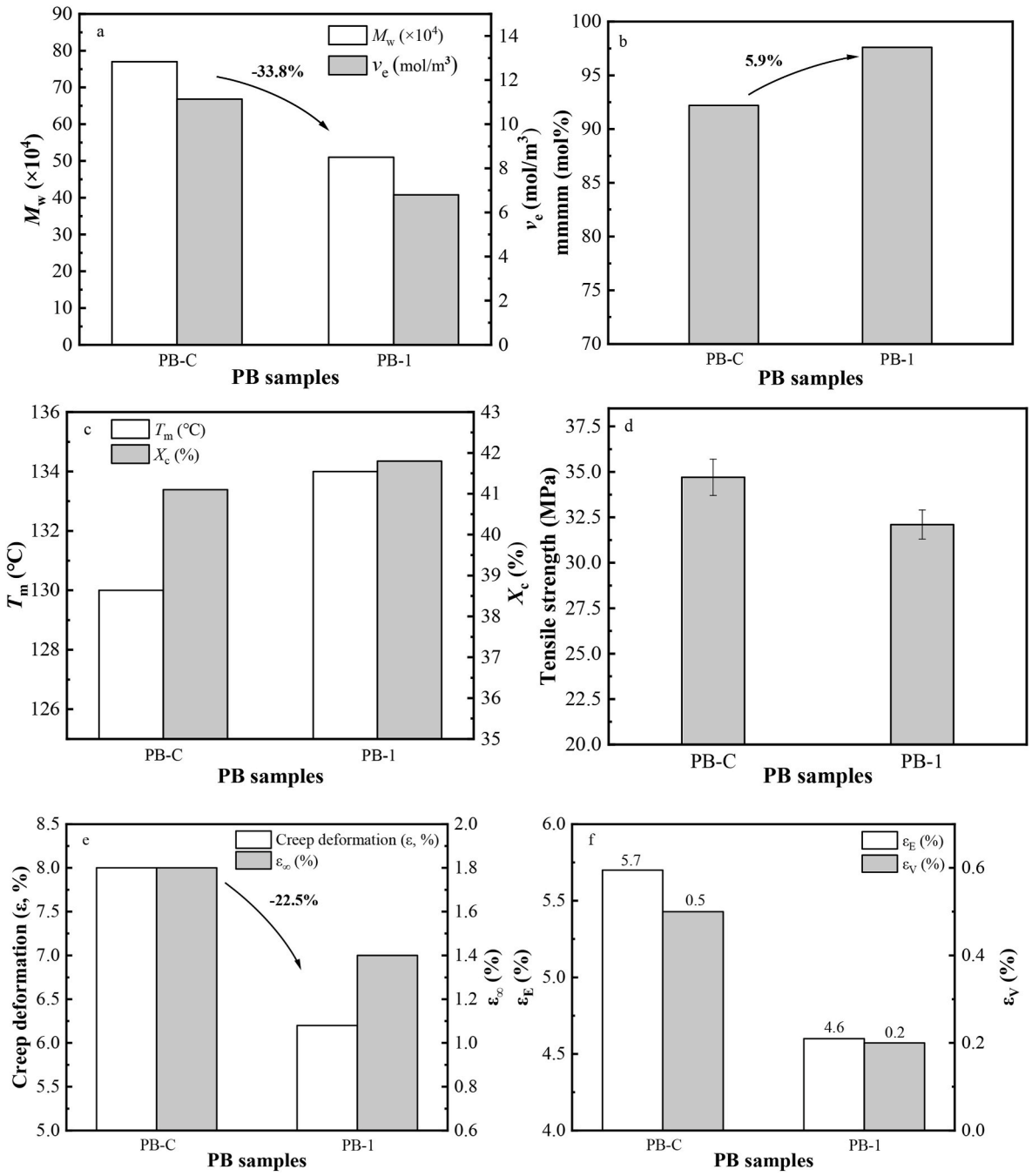

Fig. 4. (a)M_w and v_e; (b)mmmm; (c)T_m and X_c; (d)tensile strength; (e)creep deformation (ε) and ε_∞; (f)ε_E and ε_V of PB-C and PB-1.

in creep deformation and permanent creep strain (Fig. 3e) compared to PB-3. The PB-5 with v_e 28 mol/m^3 and M_w 137 × 10^4 showed tensile strength 33 MPa, creep deformation 7.7%. The PB-5 with relatively high molecular weight had more internal chain entanglements acting as amorphous domains, and inhibited the increase in crystallinity (36.9%). Anyway, the PB-5 with relatively high molecular weight showed rather high d_c and then contributed to the reduced creep deformation.

3.3. Comparison with the commercial sample PB

The commercial PB-C showed rather high isotacticity (99%), and 92.2% mmmm and 77 × 10^4 M_w. Compared with PB-C, the PB-1 had some negative factors, like relatively low M_w (Fig. 4a) and HiPB percentage, and also had positive factor like relatively high mmmm concentration (Fig. 4b). Therefore PB-1 and PB-C showed different aggregation structures (Fig. 4c) and mechanical behaviors (Fig. 4d and e). Interestingly, PB-1 presented much lower creep deformation (ε), permanent creep strain (ε_∞) (Fig. 4e), as well as much lower ε_E and ε_V (Fig. 4f). It seemed that the configurational sequence of PB-1 played more important role in the creep resistance.

3.4. Discussion

Compared with PB-2, PB-1 with 5.9% higher mmmm percentage showed 31.1% reduced creep deformation, while PB-5 with 168.6% higher M_w showed only 14.4% reduced creep deformation (Fig. 5). At the same time, compared with PB-C, although the molecular weight and HiPB fractions of PB-1 was much more lower, PB-1 with pretty high

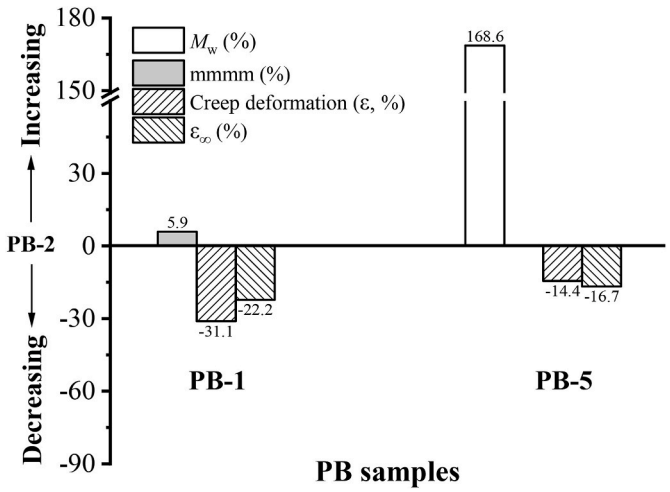

Fig. 5. Increasing or decreasing performances of PB-1 and PB-5 compared to that of PB-2.

mmmm percentage presented better creep resistance. It was deduced that the chain configurational sequences in term of mmmm percentage had greater effect on creep resistance when compared with molecular weight. The isotacticity obtained by the solvent extraction was not a good indicator to reflect the creep resistance of PB.

To further understand the influence of parameters like mmmm percentage and M_w on PB creep resistance, mmmm percentage and M_w/10000 were defined as two variates (x_1 and x_2), and correlations between creep deformation (y) and the two variates were investigated. With the help of IBM SPSS Statistics 25, the values of the two variates from PB-1 to PB-6 (Table 1) were used for data fitting to establish linear relationship between y and x. Finally, equation (7) was obtained:

$$y = 48.829–0.434x_1 - 0.003x_2 \ (R^2 = 0.970) \quad (7)$$

In which, x_1 represents mmmm percentage (mol%), x_2 represents M_w/10000, y represents creep deformation (ε, %).

Based on the obtained equation (7), it was deemed that x_1 with higher coefficient 0.434 had greater influence on y when compared to that of x_2 (0.03). Equation (7) with relatively high linear regression coeffficient (R^2 = 0.970) verified that the mmmm configurational sequence played more significant role on the creep resistance of PB when compared with molecular weight.

As Fig. 6 indicated, the molecular weight and chain microstructures influence the creep resistance of PB in different way. Increasing the molecular weight of PB led to the increase in the chain entanglements, which acted as defects restricted the formation of perfect crystals. Anyway, the increase in M_w benefited to the formation of crystals with higher d_c (PB-5, 19.1 nm). The increase in isotactic stereoregular sequence resulted in more perfect crystalline domains with less defects, which acted as the rigid crosslinking points and restricted the viscoelastic deformation of polymers. The PB form I crystals with high T_m, X_c and relative large lamellar thickness, more perfect crystal structure, presented the outstanding high-temperature creep resistance.

4. Conclusions

Both molecular weight and chain microstructures affected the thermal creep resistance of PB. PB with higher molecular weight had more larger lamellar thickness and then showed better creep resistance. While PB chains with higher mmmm concentration had more perfect chain foldings resulting in higher crystallinity and crystalline melting temperature and reduced viscoelastic behavior, and then showed excellent high-temperature creep resistance. The linear fitting further indicated that the mmmm configurational sequence played more significant role on the creep resistance of PB.

CRediT authorship contribution statement

Yuanjin Zhao: Conceptualization, Data curation, Writing-original draft. Chenguang Liu: Writing-review & editing, Validation. Huafeng Shao: Writing-review & editing, Validation. Aihua He: Funding acquisition, Supervision, Writing-review & editing.

Declaration of competing interest

The authors declare that they have no known competing financial interests or personal relationships that could have appeared to influence the work reported in this paper.

Data availability

Data will be made available on request.

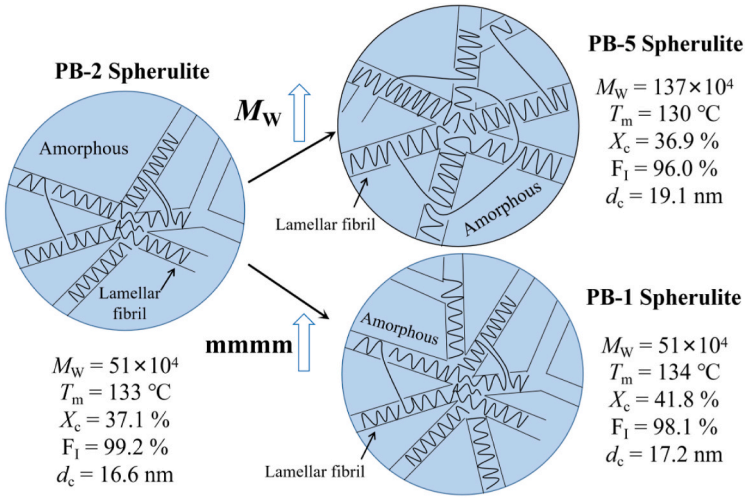

Fig. 6. Mechanism illustrations of creep resistance of polybutene-1.

Acknowledgements

This work was supported by the Major Scientific and Technological Innovation Project of Shandong Province (2021CXGC010901, 2019JZZY010352) and the Taishan Scholar Program.

References

[1] J.D. Ferry, Viscoelastic Properties of Polymer, Wiley, 1980, https://doi.org/10.6028/jres.041.008.
[2] Z.L. Hou, W.J. Wei, Market analysis for PERT floor heating tube specialty, China Synth. Resin Plast. 36 (2019) 90–93, https://doi.org/10.3969/j.issn.1002-1396.2019.02.022.
[3] R. Seguela, Critical review of the molecular topology of semicrystalline polymers: the origin and assessment of intercrystalline tie molecules and chain entanglements, J. Polym. Sci., Part B: Polym. Phys. 43 (2005) 1729–1748, https://doi.org/10.1002/polb.20414.
[4] L.J. Wang, E.G. Zou, Y.P. Wang, L. Ma, T.T. Cao, Research progress for temperature resistance polyethylene pipe resin, China Plast. Ind. 40 (2012) 1–4+13. CNKI:SUN:SLGY.0.2012-10-000.
[5] K. Feng, Q. Wang, Z.F. Li, M. Mo, Thermal oxidation stability of random copolypropylene special resin for pipes, China Synth. Resin Plast. 30 (2013) 62–64, https://doi.org/10.3969/j.issn.1002-1396.2013.04.023.
[6] R. Alaburdaitė, V. Krylova, Study of thermo-oxidative chemical pre-treatment of isotactic polypropylene, J. Therm. Anal. Calorim. 118 (2014) 1331–1338, https://doi.org/10.1007/s10973-014-4226-0.
[7] D. Bertin, M. Leblanc, S.R. A Marque, D. Siri, Polypropylene degradation: theoretical and experimental investigations, Polym. Degrad. Stabil. 95 (2010) 782–791, https://doi.org/10.1016/j.polymdegradstab.2010.02.006.
[8] P. Galli, G. Vecellio, Polyolefins: the most promising large-volume materials for the 21st century, J. Polym. Sci., Polym. Chem. Ed. 42 (2004) 396–415, https://doi.org/10.1002/pola.10804.
[9] L. Luciani, J. Seppälä, B. Löfgren, Poly-1-butene: its preparation, properties and challenges, Prog. Polym. Sci. 13 (1988) 37–62, https://doi.org/10.1016/0079-6700(88)90010-X.
[10] H.F. Shao, S.L. Wang, A.H. He, The influence of molecular weight on high shear rate macroscopic rheological properties of polybutene-1 melts through rubber-processing analyzer, Polym. Bull. 73 (2016) 3209–3220, https://doi.org/10.1007/s00289-016-1650-2.
[11] S.K. Bhateja, Uniaxial tensile creep behaviour of ultra high molecular weight linear polyethylene, Polymer 22 (1981) 23–28, https://doi.org/10.1016/0032-3861(81)90071-9.
[12] P.A. O'Connell, M.J. Bonner, R.A. Duckett, I.M. Ward, Effect of molecular weight and branch content on the creep behavior of oriented polyethylene, J. Appl. Polym. Sci. 89 (2003) 1663–1670, https://doi.org/10.1002/app.12434.
[13] G.L. Chakkalakal, C. Abetz, U. Vainio, U.A. Handge, V. Abetz, Influence of rheology and morphology on foaming of PS-*b*-PMMA diblock copolymers and their composites with modified silica nanoparticles, Polymer 54 (2013) 3860–3873, https://doi.org/10.1016/j.polymer.2013.05.025.
[14] X.B. Shi, C.L. Wu, M.Z. Rong, T. Czigany, W.H. Ruan, M.Q. Zhang, Improvement of creep resistance of polytetrafluoroethylene films by nano-inclusions, Chin. J. Polym. Sci. 31 (2013) 377–387, https://doi.org/10.1007/s10118-013-1225-8.
[15] A. Bhattacharyya, S. Chen, M. Zhu, Graphene reinforced ultra high molecular weight polyethylene with improved tensile strength and creep resistance properties, Express Polym. Lett. 8 (2014) 74–84, https://doi.org/10.3144/expresspolymlett.2014.10.
[16] A. Habas-Ulloa, J.R.M. D'Almeida, J.P. Habas, Creep behavior of high density polyethylene after aging in contact with different oil derivates, Polym. Eng. Sci. 50 (2010) 2122–2130, https://doi.org/10.1002/pen.21743.
[17] P.R. Liu, L. Peng, J.J. Chen, B. Yang, Y.N. Chen, Z.F. Luo, C.C. Han, X.B. Huang, Y. F. Men, Tensile creep failure of isotactic polypropylene under the strain criterion, Macromolecules 55 (2022) 9663–9670, https://doi.org/10.1021/acs.macromol.2c01263.
[18] I. Widiastuti, I. Sbarski, S.H. Masood, Creep behavior of PLA-based biodegradable plastic exposed to a hydrocarbon liquid, J. Appl. Polym. Sci. 127 (2013) 2654–2660, https://doi.org/10.1002/app.37575.
[19] V. Tajeddini, B.H. Atitallah, A. Muliana, Z. Ounaies, Nonlinear viscoelastic behavior of active fiber composites, J. Eng. Mater-T Asme. 136 (2014), 021005, https://doi.org/10.1115/1.4026474.
[20] Z.N. Zhang, C.Y. Tian, Z.Q. Yuan, J.J. Li, W.P. Wu, R. Xia, Temperature and loading sensitivity investigation of nanoindentation short-term creep behavior in Nafion, Mater. Res. Express 6 (2019), 055304, https://doi.org/10.1088/2053-1591/ab008b.
[21] M.W. Keller, B.D. Jellison, T. Ellison, Moisture effects on the thermal and creep performance of carbon fiber/epoxy composites for structural pipeline repair, Compos. B Eng. 45 (2013) 1173–1180, https://doi.org/10.1016/j.compositesb.2012.07.046.
[22] R.A. Arutyunyan, Creep fracture of nonlinear viscoelastic media undergoing UV radiation, Int. J. Fract. 132 (2005) L3–L8, https://doi.org/10.1007/s10704-005-0023-x.
[23] D. Maring, M. Wilhelm, H.W. Spiess, B. Meurer, G. Weill, Dynamics in the crystalline polymorphic forms I and II and form III of isotactic poly-1-butene, J. Polym. Sci., Polym. Phys. Ed. 38 (2000) 2611–2624, https://doi.org/10.1002/1099-0488(20001015)38:20<2611::AID-POLB10>3.0.CO;2-E.
[24] F. Danusso, G. Gianotti, The three polymorphs of isotactic polybutene-1: dilatometric and thermodynamic fusion properties, Macromol. Chem. Phys. 61 (1963) 139–156, https://doi.org/10.1002/macp.1963.020610113.
[25] B. Lotz, A. Thierry, Spherulite morphology of form III isotactic poly(1-butene), Macromolecules 36 (2003) 286–290, https://doi.org/10.1021/ma021452u.
[26] X. Qiu, C.L. Hu, J.Q. Li, D.H. Huang, S.C. Jiang, Role of conformation in crystal formation and transition of polybutene-1, CrystEngComm 21 (2019) 4243–4249, https://doi.org/10.1039/C9CE00576E.
[27] A.H. He, C.S. Xu, H.F. Shao, Y. Wei, B.C. Huang, Effect of molecular weight on the polymorphic transformation of isotactic poly (1-butene), Polym. Degrad. Stabil. 95 (2010) 1443–1448, https://doi.org/10.1016/j.polymdegradstab.2010.06.027.
[28] H.F. Shao, Y.P. Ma, H.R. Nie, A.H. He, Solvent vapor annealing induced polymorphic transformation of polybutene-1, Chin. J. Polym. Sci. 34 (2016) 1141–1149, https://doi.org/10.1007/s10118-016-1823-3.
[29] Y.P. Ma, W.P. Zheng, C.G. Liu, H.F. Shao, H.R. Nie, A.H. He, Differential polymorphic transformation behavior of polybutene-1 with multiple isotactic sequences, Chin. J. Polym. Sci. 38 (2020) 164–173, https://doi.org/10.1007/s10118-020-2337-6.
[30] Y.N. Qiao, Q. Wang, Y.F. Men, Kinetics of nucleation and growth of form II to I polymorphic transition in polybutene-1 as revealed by stepwise annealing, Macromolecules 49 (2016) 5126–5136, https://doi.org/10.1021/acs.macromol.6b00862.
[31] F. Azzurri, A. Flores, G.C. Alfonso, F.G.B. Calleja, Polymorphism of isotactic poly(1-butene) as revealed by microindentation hardness. 1. Kinetics of the transformation, Macromolecules 35 (2002) 9069–9073, https://doi.org/10.1021/ma021005e.
[32] B.H. Wang, K.Z. He, Y.G. Lu, Y.F. Zhou, J.L. Chen, C.G. Shen, J.B. Chen, Y.F. Men, B. Zhang, Nucleation mechanism for form II to I polymorphic transformation in polybutene-1, Macromolecules 53 (2020), https://doi.org/10.1021/acs.macromol.0c00885.
[33] Y.A. Qin, V. Litvinov, W. Chassé, B. Zhang, Y.F. Men, Change of lamellar morphology upon polymorphic transition of form II to form I crystals in isotactic Polybutene-1 and its copolymer, Polymer 215 (2020), 123355, https://doi.org/10.1016/j.polymer.2020.123355.
[34] L. Bove, M.R. Nobile, Shear flow effects on polymer melts crystallization: kinetics features, Macromol. Symp. 180 (2002) 169–180, https://doi.org/10.1002/1521-3900(200203)180:13.0.CO;2-A.
[35] R.L. Combs, D.F. Slonaker, H.W. Coover, Effects of molecular weight distribution and branching on rheological properties of polyolefin melts, J. Appl. Polym. Sci. 13 (1969) 519–534, https://doi.org/10.1002/app.1969.070130312.
[36] S. Acierno, N. Grizzuti, H.H. Winter, Effects of molecular weight on the isothermal crystallization of poly(1-butene), Macromolecules 35 (2002) 5043–5048, https://doi.org/10.1021/ma0200423.
[37] H.F. Shao, W. Yao, B.C. Huang, Y.X. Zhao, Effect of crystallinity and spherulite structure on the mechanical properties of poly(1-butene), J. Polym. Eng. 29 (2009) 341–354, https://doi.org/10.1515/POLYENG.2009.29.6.341.
[38] H.F. Shao, D.X. Jiang, M.M. Zhang, W. Yao, B.C. Huang, Characterization of the polymorphic transformation of poly(1-butene) based on FTIR and mechanical properties, J. Polym. Res. 19 (2012) 1–6, https://doi.org/10.1007/s10965-012-9919-0.
[39] W.P. Zheng, M.C. Han, Y.J. Zhao, H.F. Shao, A.H. He, An improved method for the high isotacticity measurement of polybutene-1, Polym. Test. 94 (2020), 107011, https://doi.org/10.1016/j.polymertesting.2020.107011.
[40] Y.N. Qiao, H. Wang, Y.F. Men, Retardance of form II to form I transition in polybutene-1 at late stage: a proposal of a new mechanism, Macromolecules 51 (2018) 2232–2239, https://doi.org/10.1021/acs.macromol.7b02481.
[41] T. Deplancke, O. Lame, F. Rousset, I. Aguili, R. Seuela, G. Vigier, Diffusion versus cocrystallization of very long polymer chains at interfaces: experimental study of sintering of UHMWPE nascent powder, Macromolecules 47 (2013) 197–207, https://doi.org/10.1021/ma402012f.
[42] P. Dong, K. Wang, F.J. Li, Q. Fu, Chain entanglement regulation of sintered ultrahigh molecular weight polyethylene and its effect on properties, Acta Polym. Sin. 51 (2020) 9, https://doi.org/10.11777/j.issn1000-3304.2020.191598.
[43] B.Y. Wu, Y.D. Cai, X.W. Zhao, Y. Lin, Fabrication of well-miscible and highly enhanced polyethylene/ultrahigh molecular weight polyethylene blends by facile construction of interfacial intermolecular entanglement, Polym. Test. 93 (2021), 106973, https://doi.org/10.1016/j.polymertesting.2020.106973.
[44] W.P. Zheng, A.H. He, C.G. Liu, H.F. Shao, R.G. Wang, The influences of alkylaluminium as cocatalyst on butene-1 polymerization with $MgCl_2$-supported $TiCl_4$ Ziegler-Natta catalysts, Polymer 210 (2020), 122998, https://doi.org/10.1016/j.polymer.2020.122998.
[45] W.P. Zheng, Y.J. Zhao, M.C. Han, C.S. Zhou, A.H. He, Regulation of alkoxysilane on stereoregular polymerization of Butene-1 catalyzed by $TiCl_4/MgCl_2$ Ziegler-Natta catalysts, Polymer 228 (2021), 123925, https://doi.org/10.1016/j.polymer.2021.123925.
[46] X.B. Jiang, A.H. He, Stereospecific polymerization of olefins with supported Ziegler-Natta catalysts, Polym. Int. 63 (2014) 179–183, https://doi.org/10.1002/pi.4633.
[47] I.M. Word, J. Sweeney, Mechanical Properties of Solid Polymers, Wiley, 1983, https://doi.org/10.1002/9781119967125.
[48] Y. Jia, Z.M. Jiang, X.L. Gong, Z. Zhang, Creep of thermoplastic polyurethane reinforced with ozone functionalized carbon nanotubes, Express Polym. Lett. 6 (2012) 750–758, https://doi.org/10.3144/expresspolymlett.2012.80.